Electron spin dynamics in nanodevices and geometrical effects

D. Giuliano [1,2], P. Lucignano [1,3,4], A. Tagliacozzo [1,3]

[1] *Dipartimento di Scienze Fisiche Università degli studi di Napoli "Federico II ", Napoli, Italy*

[2] *Dipartimento di Fisica, Università della Calabria and I.N.F.N., Gruppo collegato di Cosenza, Arcavacata di Rende, I-87036, Cosenza, Italy*

[3] *Coherentia-INFM, Monte S.Angelo – via Cintia, I-80126 Napoli, Italy*

[4] *SISSA and INFM Democritos National Simulation Center, Via Beirut 2–4, 34014 Trieste, Italy*

We discuss nonlocal quantum mechanical effects in mesoscopic devices, for studying which, path integral has been shown to provide quite a powerful and compact approach. In particular, we focus onto geometrical phase effects. As a former example, we discuss how a geometrical phase due to spin-orbit coupling may affect Aharonov–Bohm conductance oscillations in a mesoscopic ring. As a latter example, we show that a pertinent cycling in parameter space may induce a robust Berry phase in a quantum dot tuned close to a three-level degeneracy. In both cases, we propose to detect geometrical phase effects by means of an appropriate DC transport measurement.

1 Introduction

Nowadays, it is possible to manipulate the wavefunction of the electrons in a nanodevice, without letting it lose coherence. Of course, "taming" decoherence is possible only when operating devices of nanometric dimensions. This can be practically realized by adiabatically tuning gate voltages, or magnetic fields applied to the system. Indeed, the Aharonov–Bohm (AB) effect has been mostly used to coherently modulate the electron wavefunction. Also, recently people are achieving good qualitative control on the interaction between gates and the underlying electron spins in semiconductor heterostructures.

In this framework, path integral formalism is particularly suitable, in order to discuss quantum interference in mesoscopic systems, as it allows for a straightforward analysis of nonlocal effects in the electron quantum propagator, which are at the hearth of quantum interference.

In these notes we report on results obtained in two different systems:

a) Modulation of the current due to spinful electrons transmitted ballistically across a mesoscopic ring under the influence of orthogonal stationary electric and magnetic fields.

b) Study of a peculiar Berry phase that can be added to the interacting electrons of a Quantum Dot (QD) close to a level crossing.

In particular, in section 2 we discuss the path integral formulation of the device at point a). This allows us to make it explicit that interference is due to the combined effects of a Berry phase, arising from the spin-orbit interaction, of the Aharonov–Bohm phase and of the Zeeman spin splitting. Instead, in Section 3 we

add by hand a Berry phase to an isolated dot, by cycling an electric field orthogonal to the dot plane, close to a level crossing in parameter space. We shortly address the problem of the of the read-out of the phase.

2 Quantum propagator of spinful electrons in an interferometric ring

An interferometric ring realized on a solid state substrate, has typical size of the order of the coherence length of electrons within the substrate. In this case, one can apply contacts to opposite ends of the ring and use the device for generating and detecting interference effects between electrons undergoing different paths in space [1]. A typical, and well known, phenomenon is the Aharonov–Bohm phase, picked up by electrons when they travel along a closed path in space pierced by a nonzero magnetic flux [2]. In addition to the AB phase, spinful particles suffer another mechanism that may possibly generate quantum interference. Indeed, spin orbit interaction (SOI) in mesoscopic devices may give rise to an additional effective field, which provides a geometrical contribution to the electron wavefunction phase, in addition to the BA phase (Rashba effect) [3]. Rashba effect can be tuned by properly acting on the device with external potential gates. We will show that, in the limit in which the spin dynamics due to SOI is "adiabatic", with respect to orbital motion of the electrons in the ring, the corresponding accumulated phase takes the form of an adiabatic, su(2)-Berry phase. In order to show this features, let us start with the description of the electron dynamics across the interferometric ring. By neglecting interaction effects among electrons, we formulate a description of the relevant physics of the system within an appropriate, single particle, path integral formulation.

Despite its apparent simplicity, we will show that such a formulation embodies all the relevant phenomenology.

The interferometric ring (of radius R) is assumed to lie on a plane, of coordinates x and y. An external magnetic field B is applied, orthogonal to the plane. B is described by the vector potential $\vec{A}$, lying within the (x,y)-plane. An applied electric field E tunes α, the SOI strength . $\vec{S}$ is the electron spin so that, if ω_c is the cyclotron frequency and the Zeeman spin splitting is included, the total Hamiltonian for an electron in the ring is given by

$$H = \frac{1}{2m}\left(\vec{p} + \frac{e}{c}\vec{A}\right)^2 + \frac{\alpha}{\hbar}\left[\left(\vec{p} + \frac{e}{c}\vec{A}\right)\times\vec{S}\right]\cdot\hat{z} + \frac{\hbar\omega_c}{2}S^z\,. \tag{1}$$

Since we want to resort to a path integral formulation of the problem, we need to get back to the Lagrangian of the system. This is obtained by Lagrange transforming H and is given by

$$\mathcal{L} = \frac{m}{2}|\vec{v}|^2 - \frac{e}{c}\vec{v}\cdot\vec{A} + \frac{m\alpha}{\hbar}\left[\vec{v}\times\vec{S}\right]\cdot\hat{z} - \frac{\hbar\omega_c}{2}S^z\,, \tag{2}$$

where $\vec{v}$ is the electron velocity. The Lagrangian in Eq.(2) will be the starting point for the path integral formulation of the theory.

To compute the DC conductance across the ring, one needs the single electron transmission amplitude $A(\sigma_f, \sigma_i|E_F)$ for an electron entering the ring with spin σ_i and getting out with spin σ_f, at the Fermi energy E_F. Within Landauer's approach [4], the total DC conductance across the ring is, therefore, given by

$$G = \frac{e^2}{h} \sum_{\sigma_i, \sigma_f} \left| A(\sigma_f, \sigma_0|E_F) \right|^2 . \tag{3}$$

In a quasi one-dimensional ring the only orbital coordinate for the particle is an angle φ along the circle.

In [5], we express the amplitudes as path integrals over the orbital coordinate only, by treating spin coordinates as operators. The final result is, therefore, a matrix in spin space, whose entries are just the $A(\sigma, \sigma'|E_F)$ in Eq.(3).

For simplicity, let us assume symmetric boundary conditions, that is, since we are only interested in electrons transmitted across the ring, we will assume that the electron enters the ring at $\varphi(0)$, makes a certain number $(2n+1,\, n = 0, \pm 1, \pm 2, \ldots)$ of half turns, and exits at $\varphi(t_f) = (2n+1)\pi + \varphi(0)$. If σ_0 is the initial spin polarization of the dot and σ_f is the final spin polarization, the corresponding amplitude is given by

$$A\big(\sigma_f, (2n+1)\pi+\varphi(0), t_f|\sigma_0, \varphi(0), 0\big) = \int_{\varphi(0)}^{(2n+1)\pi+\varphi(0)} \mathcal{D}\varphi \left\langle \sigma_f, t_f | \mathrm{e}^{\mathrm{i}S[\varphi,\vec{\sigma}]} \right| \sigma_0 \Big\rangle, \tag{4}$$

where [5]

$$\begin{aligned} S[\varphi, \vec{\sigma}] = \int_0^{t_f} \mathrm{d}t \Bigg\{ & \frac{mR^2}{2} (\dot{\varphi})^2 - \hbar \frac{\phi}{\phi_0} \dot{\varphi} + \frac{\alpha^2 m}{2\hbar^2} + \frac{\hbar^2}{8mR^2} - \\ & - \left[\frac{\hbar\omega_c}{2} \sigma^z + \frac{\alpha R m \dot{\varphi}}{\hbar} \left(\mathrm{e}^{-\mathrm{i}\varphi} \sigma^+ + \mathrm{e}^{\mathrm{i}\varphi} \sigma^- \right) \right] \Bigg\}. \end{aligned} \tag{5}$$

and $(\sigma^z, \sigma^\pm)$ are Pauli matrices.

In order for the electron to enter the ring at $\varphi(0)$, to perform $2n+1$ half-turns and go outside of the ring at the opposite contact, it has to be reflected at any connection between ring and leads $2|n|-2$ times, and transmitted twice. Therefore, if $\bar{r}$ is the reflection amplitude at any contact, and $\bar{t}$ is the transmission amplitude, the total amplitude for the electron at energy E_F will be given by

$$\begin{aligned} A(\sigma_f, \sigma_0|E_F) = |\bar{t}|^2 \sum_{n=-\infty}^{\infty} \int_0^{\infty} & \mathrm{d}t_f \, (\bar{r})^{2(|n|-1)} \exp\left(\mathrm{i} \frac{E_F t_f}{\hbar} \right) \times \\ & \times A\big(\sigma_f, (2n+1)\pi + \varphi(0), t_f|\sigma_0, \varphi(0), 0\big) . \end{aligned} \tag{6}$$

Transmission is elastic and ballistic. We fix the energy of the incoming electron at the Fermi threshold, what requires Fourier transforming with respect to the final time t_f.

The amplitude in Eq.(6) appears as a sum over different "topological sector", each one characterized by the integer n. To proceed in calculating the amplitude,

we choose to perform a saddle point approximation on the orbital path of the particle and to treat the spin dynamics exactly.

Saddle point equations are the motion equation of the particle and of its spin and they are entangled. It follows that, to solve for the classical orbiting trajectory of the particle we have to write the full set of saddle point equations including those referring to the semiclassical spin dynamics.

The Haldane's mapping [6] allows us to account properly for the explicit dependence of $\mathcal{L}$ of Eq.(2) on the spin coordinates. Here, we just provide the recipe for expressing real time amplitudes as path integrals in real time.

First of all, let s be the total "length" of the spin (in our case, $s = \frac{1}{2}$); Φ and Θ are its polar angles in spin space. The full action for the problem becomes [6]:

$$S = \int \mathrm{d}t \Big\{ \frac{mR^2}{2} (\dot{\varphi})^2 - \hbar \frac{\phi}{\phi_0} \dot{\varphi} - s \frac{\hbar \omega_c}{2} \cos(\Theta) - \\ - s \frac{\alpha m R}{\hbar} \dot{\varphi} \sin(\Theta) \cos(\Phi - \varphi) + s \dot{\Phi} \cos(\Theta) + \frac{m \alpha^2}{\hbar^2} \Big\}. \tag{7}$$

Classical trajectories are obtained by solving Lagrange equations for the coordinates $\varphi(t)$, $\Phi(t)$, $\Theta(t)$ derived from Eq.(7):

$$\begin{aligned} &\frac{\delta S}{\delta \varphi} = 0 \Rightarrow m R^2 \ddot{\varphi} = 0 \,, \\ &\frac{\delta S}{\delta \Phi} = 0 \Rightarrow \sin(\Theta) \left[\dot{\Theta} + \frac{\alpha m R}{\hbar} \dot{\varphi} \sin[\Phi - \varphi] \right] = 0 \,, \\ &\frac{\delta S}{\delta \Theta} = 0 \Rightarrow \sin\Theta \left(\dot{\Phi} + \frac{\hbar \omega_c}{2} \right) + \frac{\alpha m R}{\hbar} \cos\Theta \cos(\Phi - \varphi) = 0 \,. \end{aligned} \tag{8}$$

Eqs.(8) implies that $\dot{\varphi} = \dot{\varphi}_0 =$ constant, along classical trajectories. It can be shown that the Eqs.(8) describe the precession of a classical spin along the direction of a time dependent magnetic field. The classical dynamics of the spin can be studied by substituting $\varphi(t)$ with $\dot{\varphi}_0 t + \varphi_0$, and by solving the corresponding system of first-order differential equations for $\Theta(t)$ and $\Phi(t)$.

In what follows we will only use the first of Eqs.(8), which shows that, in the classical limit, the orbital dynamics does not depend on the spin dynamics.

Next we expand the path integral up to second order in the deviations from the classical solution for the orbital equation of motion within the n^{th} topological sector:

$$\varphi_n(t) = \varphi(0) + \mathrm{sgn}(n) \pi (2|n| - 1) \left(\frac{t}{t_f} \right). \tag{9}$$

Insertion of Eq.(9) into Eq.(6), gives, after the gaussian integration over final times has been performed, the approximated transmission amplitude at fixed spin polar-

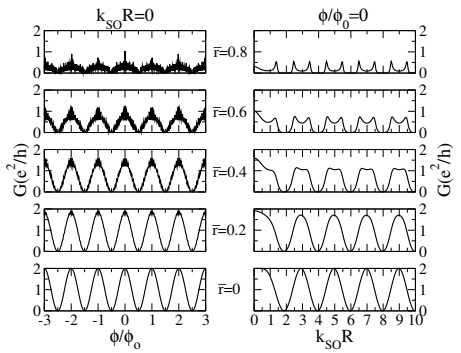

Fig. 1. DC conductance across the ring vs. ϕ/ϕ_0 at $k_{\rm SO}R = 0$ (left panel); ring's DC conductance vs. $k_{\rm SO}R = 0$ at $\phi/\phi_0 = 0$.

izations at energy E_F:

$$A(\sigma_f,\sigma_0|E_F) = \sqrt{\frac{m}{2\tilde{E}_0}}\,|\bar{t}|^2 \sum_{n\neq 0, n=-\infty}^{\infty} \left\{ (\bar{r})^{2(|n|-1)} \exp\left[\mathrm{i}\,\frac{mR^2}{2\hbar t_n}\left(\pi(2|n|-1)\right)^2 \right] \times \right.$$
$$\times \exp\left[-\mathrm{i}\,\frac{\phi}{\phi_0}\left(\pi(2|n|-1)\right)\mathrm{sign}(n) \right] \exp\left[\mathrm{i}\,\frac{E_F t_n}{\hbar} \right] \times$$
$$\left. \times \exp\left[\mathrm{i}\left[1+(k_{\rm SO}R)^2\right]\frac{t_n}{16\tau_0} \right] \right\} \left\langle \sigma_f | \hat{U}_{\rm cl}(t_n,0) | \sigma_0 \right\rangle , \tag{10}$$

with $\tilde{E}_0 = E_F + \dfrac{\hbar[1+(k_{\rm SO}R)^2]}{16\tau_0}$, $\tau_0 = \dfrac{mR^2}{2\hbar}$, $k_{\rm SO}R = \dfrac{4\alpha\tau_0}{\hbar R}$.

The effective propagation matrix in spin space, $U_{\rm cl}(t,t')$, is defined as

$$U_{\rm cl}(t,t') = \hat{T}\left\{ \exp\left[-\frac{\mathrm{i}}{\hbar}\int_{t'}^{t} \mathrm{d}\tau\, \vec{b}(\tau)\cdot\vec{\sigma} \right] \right\}, \tag{11}$$

($\hat{T}$ is the time ordering operator) and the effective time dependent magnetic field seen by the electron spin is

$$\vec{b}(t) \equiv (b^z, b^+, b^-) = \left(\frac{\hbar\omega_c}{2}, k_{\rm SO}R\hbar\dot{\varphi}_n \mathrm{e}^{\mathrm{i}\varphi_n(t)}, k_{\rm SO}R\hbar\dot{\varphi}_n \mathrm{e}^{-\mathrm{i}\varphi_n(t)} \right). \tag{12}$$

The amplitudes of Eq.(10) have been numerically calculated in Ref. [5], and have accordingly been used to compute the DC conductance from Landauer's formula. The results are shown in Figs.(1, 2).

In Fig.1, we report oscillations in the DC conductance across the ring as a function of ϕ/ϕ_0, and of $k_{\rm SO}R$, for different values of the reflection amplitude at the contacts, $\bar{r}$.

In the left panel, we show AB oscillations vs. ϕ/ϕ_0. For $\bar{r} > 0$, interference effects appear, due to sectors with winding numbers $|n+\frac{1}{2}| > 1$. We see that,

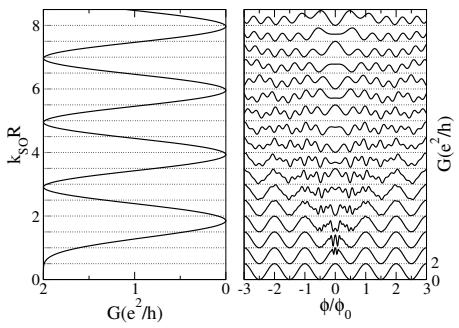

Fig. 2. DC conductance across the ring vs. $k_{\rm SO}R$ at $\phi/\phi_0 = 0$ (left panel); DC conductance vs. ϕ/ϕ_0 at increasing value of SOI.

as $\bar{r}$ increases, the conductance is reduced, except when the constructive interference condition is fulfilled, that is, when ϕ/ϕ_0 is close to an integer value. In the right panel, we plot the conductance vs. $k_{\rm SO}R$ at $\phi/\phi_0 = 0$, for increasing $\bar{r}$. In the case of ideal coupling, $\bar{r} = 0$, oscillation of the conductance reveal the localization/antilocalization conditions, due to spin orbit coupling, that is expected in mesoscopic structures [7,8]. As seen in the figure,multiple reflections do not induce higher harmonics in the localization, but an enhancement in the damping.

In the right panel of Fig.(2), we plot the conductance as a function of ϕ/ϕ_0 at $\tilde{E}_0 = 0$ and $\bar{r} \sim 0$ for different values of $k_{\rm SO}R$ (For reference, in the left panel we show the DC conductance *vs.* $k_{\rm SO}R$ at $\phi = 0$). The overall agreement with the experimental data leads us to the conclusion that, in real samples the coupling between the contacts and the leads is approximately ideal ($\bar{r} \sim 0$). The change in periodicity of the oscillations at increasing $k_{\rm SO}R$ is evident.

To understand the emerging periodic structure of the Berry phase oscillations, in Ref. [5] we performed the Fourier transform of the DC conductance across the ring for different values of SOI strength. The result is that, as soon as SOI is turned on, several structures appear, on top of the fundamental peak, due to Aharonov–Bohm oscillations. For small values of SOI, two satellite peaks arise. These two peaks, together with the Aharonov–Bohm central peak, eventually evolve into a four peak structure, for large SOI. In order to qualitatively understand such a behavior, we may consider the expansion of the formula for the conductance, within adiabatic approximation ($k_{\rm SO}R\dot{\varphi} \ll \omega_c$). We obtain

$$\sum_{\sigma\sigma'} |A(\sigma;\sigma')|^2 \approx 2 - 2\sum_{\pm}\left\{\cos^2\chi\cos\left[2\pi\frac{\phi}{\phi_0} \pm \pi\cos\chi\right] + \sin^2\chi\cos\left[\pi\frac{\phi}{\phi_0} \pm \frac{\pi\omega_c}{\dot{\varphi}}\right]\right\}, \tag{13}$$

where $\cos\chi = \left[1 + (k_{\rm SO}R\dot{\varphi}/\omega_c)^2\right]^{-1/2}$.

Eq.(13) gives back simple AB oscillations when there is no SOI. For small spin orbit coupling, $\sin(\chi)$ becomes $\neq 0$, while $\cos(\chi)$ is still ~ 1. Therefore, the latter term in Eq.(13) gives rise to satellite frequencies, as $\omega_c/\dot{\varphi} \propto \phi/\phi_0$. When SOI

increases, $\cos(\chi)$ itself becomes $\propto \phi/\phi_0$, and a four-peak structure develop, which is a signature of Berry phase [5,9,10]. Dephasing effects are discussed in Ref. [5].

3 Three-level avoided crossing in a Quantum Dot and Berry phase

In this Section we show that it is possible to add a special type of Berry phase to the many-electron wavefunctions, describing interacting electrons in a QD, by adiabatically cycling voltages applied to the gates, when the dot is tuned close to accidental degeneracy points of the energy spectrum.

The device we focus onto is a vertical quantum dot (QD), disk-shaped in the (x, y)-plane, with applied external electric and magnetic fields, orthogonal to the dot's plane. At this stage of the derivation, we assume the dot to be isolated, that is, it is not connected to any metallic lead. The applied field can be tuned, in order to get control on the added phase. In particular, both the applied magnetic field B and electric field $\mathcal{E}$ are directed along the z-axis. B is uniform, while $\mathcal{E}$ takes a small angular modulation as

$$\mathcal{E} = e + g_1 \cos(\theta) + g_2 \sin(\theta)\,, \tag{14}$$

where ρ and θ are the polar coordinates on dot's plane.

In the following, we take g_1 and g_2 to be equal to the real, and to the imaginary part of a complex number g, respectively.

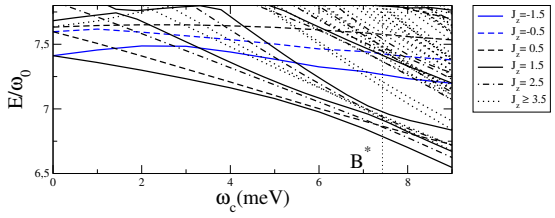

Fig. 3. Level structure of the three-electron quantum dot for $B \sim B^* \sim 6\,\mathrm{meV}$. Relevant levels in this paper are the lower two ones at $J = \frac{3}{2}$ (full line) and the one at $J = \frac{5}{2}$ (broken-dotted line)

In Fig. 3, we report the levels vs magnetic field B for a dot with $N = 3$ interacting electrons, including spin-orbit coupling. In the following, we focus on the first avoided crossing at low energy, taking place at $\omega_c \approx 6\,\mathrm{meV}$, which corresponds to an applied field $B = B_*$. The total angular momentum of the states $J_z = M + S_z$ is marked aside and used to label the states. We use a short notation for the Slater determinants of low J which contribute to these states. The locations in the state follow the natural sequence of single particle orbital quantum numbers: $(n, m = n) = (0,0)$, $(1,1)$, $(2,2)$, separated by commas. In the presence of a magnetic field, we take $m = n$ as always favored, with respect to $m \in (-n, \ldots, n-1)$. Let us now analyze the most relevant Slater determinants which contribute to the states with $J = \frac{3}{2}$ (full lines). The orientation of the electron spin is labeled by

$u =\uparrow$, $d =\downarrow$. Both ud at the same location imply double occupancy of the same orbital with opposite spins. A zero at any location indicates that the corresponding orbital is empty.

At zero magnetic field the lowest state in energy, which we denote by $|\frac{3}{2}, o\rangle$, is mostly $|d, ud, 0\rangle$, because the e–e interaction disfavors double occupancy of the $n = 0$ level, which has an "s"-like single particle orbital. The next one, $|\frac{3}{2}, -\rangle$ is mostly $|ud, u, 0\rangle$, but it soon turns into $|d, d, d\rangle$, upon increasing B, with some nonzero component on $|ud, u, 0\rangle$, as the avoided crossing at $\omega_c \approx 1.5$ is approached. There is one more relevant state in the middle of the gap (broken-dotted line), denoted by $|J = \frac{5}{2}\rangle$ in the following, of the kind $|d, u, d\rangle$.

At the level crossing near $\omega_c = 6\,\mathrm{meV}$, the electric field Eq.(14) couples the states $|\frac{3}{2}, o\rangle$, $|\frac{5}{2}\rangle$ and $|\frac{3}{2}, -\rangle$ with each other (there is another state with $J = \frac{1}{2}$ in the gap (broken line) which is not coupled to the remaining ones: therefore, we will neglect it in the following). Before the crossing, the states $|\frac{3}{2}, o\rangle$ and $|\frac{3}{2}, -\rangle$ mostly possess $|d, ud, 0\rangle$ and $|d, d, d\rangle$-character, respectively. After the crossing, they swap with each other.

The isotropic spin-orbit interaction $\hat{e}$ couples the states $|\frac{3}{2}, i = o, -\rangle$ with each other, as they belong to the same J. On the other hand, the matrix elements of the g-terms between single particle orbitals with orbital z-components of the angular momenta equal to m, m', and spin equal to σ, σ', are non zero for $m = m'$ or $m = m' + 2$, provided that $\sigma' = -\sigma$. The relevant amplitudes take the form

$$\begin{aligned} A_{n'm'+,nm-} &= \langle n'm'|\,\rho\,\sin\theta \mathrm{e}^{-\mathrm{i}\theta}(\partial_\rho + \frac{m}{\rho})|nm\rangle = \\ &= \frac{1}{\mathrm{i}}\left(\delta_{m'+2,m} - \delta_{m',m}\right) \times \frac{1}{2}\int_0^\infty \sqrt{t}\,\mathrm{d}t\, R_{n'|m'|}(t)\left(2\sqrt{t}\partial_t + \frac{m}{\sqrt{t}}\right) R_{n|m|}(t)\,, \end{aligned} \tag{15}$$

where $R_{n'|m'|}(t)$ are the radial solutions of the $2-d$ harmonic oscillator expressed in terms of Laguerre polynomials

$$R_{n|m|}(t) \propto \mathrm{e}^{-t/2}\, t^{|m|/2}\, L^{|m|}_{(n-|m|)/2}(t)\,.$$

Here $t = \rho^2/l^2$, where $l = \sqrt{\hbar/m\omega_0}$, $\omega_0 = \sqrt{\omega_d^2 + \omega_c^2/4}$, [5].

Hence, the non zero matrix elements of $\hat{g}$ are $M_1 = \langle d, u, d|\hat{g}|d, d, d\rangle$ and $M_2 = \langle d, u, d|\hat{g}|ud, u, 0\rangle$. It follows that $\hat{g}$ couples $|\frac{3}{2}, -\rangle$ with $|\frac{5}{2}\rangle$, but it does not significantly couple $|\frac{3}{2}, o\rangle$ to $|\frac{5}{2}\rangle$.

At $b > 0$ the order is reversed: the state with $i = o$ is the lowest one in energy, and it is mostly $|d, d, d\rangle$. The middle one is still $|\frac{5}{2}\rangle$, while the highest energy state, $|\frac{3}{2}, -\rangle$, is mostly $|d, ud, 0\rangle$.

Near the three-level degeneracy, once restricted to the "physical" space spanned by the three states above, turns out to be: (up to a term, proportional to the identity matrix)

$$h[b, g_1, g_2, e] = \begin{bmatrix} -b & 0 & g^* \\ 0 & 2b & e \\ g & e & -b \end{bmatrix}, \tag{16}$$

where $b \propto (B - B_*)$ parametrizes the "distance" from the degeneracy point.

In the next section, we show that, upon properly cycling the parameters in the truncated Hamiltonian, it is possible to generate a peculiar type of Berry phase, at the quantum dot.

4 Truncated Hamiltonian and adiabatic phase

It is possible to fully decompose the matrix h in the basis of su(3) generators, as

$$h = \left(-\frac{3}{2}\, b\right) \mathbf{T}_3 + \left(\frac{\sqrt{3}}{2}\right) \mathbf{T}_8 + g_1 \mathbf{T}_4 + g_2 \mathbf{T}_5 + e\mathbf{T}_6\,, \tag{17}$$

where the su(3) generators are reported in appendix.

In the following, we will denote by $\vec{\lambda}$ the set of parameters that define the linear combination of Gell-Mann generators. In paricular, from Eq.(17) we get:

$$(\lambda_1, \lambda_2, \lambda_3, \lambda_4, \lambda_5, \lambda_6, \lambda_7, \lambda_8) = \left(0, 0, -\frac{3}{2}\, b, g_1, g_2, e, 0, \frac{\sqrt{3}}{2}\, b\right). \tag{18}$$

The eigenvalues of h are simply expressed in terms of the coordinates R and Ψ, given by

$$R = \sqrt{b^2 + \frac{e^2 + |g|^2}{3}}\,, \quad \sin(3\Psi) = -\frac{b(b^2 + \frac{1}{2}\, e^2 - |g|^2)}{R^3}\,. \tag{19}$$

In decreasing order, the energy eigenvalues are given by

$$E_\ell = 2R \sin\left[\Psi + \tfrac{2}{3}\,(\ell - 1)\pi\right]. \tag{20}$$

The corresponding eigenvectors $|e_\ell, \vec{\lambda}\rangle$ are expressed as three-component column vectors as ($\vec{\lambda}$ are the parameters of the Hamiltonian h)

$$\left|e_\ell, \vec{\lambda}\right\rangle = C_\ell \begin{bmatrix} g^* \\ -e\,\dfrac{b + E_\ell}{2b - E_\ell} \\ b + E_\ell \end{bmatrix}, \tag{21}$$

where $C_\ell = \left(|g|^2 + e^2 \left(\dfrac{b + E_\ell}{2b - E_\ell}\right)^2 + (b + E_\ell)^2\right)^{-1/2}$.

We now imagine of performing an adiabatic modulation of the parameters of h. In particular, we will keep b and e constant, and will make the parameter g adiabatically evolve as $g \to g\mathrm{e}^{\mathrm{i}\omega t}$. This corresponds, for instance, to applying an electric field depending on both space and time of the form

$$\mathcal{E} = e + g\left[\mathrm{e}^{\mathrm{i}\pi/4} \cos\left(\theta - \frac{2\pi t}{T}\right) + \mathrm{e}^{-\mathrm{i}\pi/4} \cos\left(\theta + \frac{2\pi t}{T}\right)\right], \tag{22}$$

where T is the cycling period.

Because some of its parameters have become explicitly dependent on time, the Hamiltonian itself will be dependent on time t. Accordingly, the "adiabatic" basis $|e_\ell, \vec{\lambda}\rangle$ will take an explicit dependence on time, $|e_\ell, t\rangle$. The states $|e_\ell, t\rangle$ are periodic in t, with period equal to T. Although the states $|e_\ell, \vec{\lambda}\rangle$ are now explicitly dependent on time, still, at any t, they provide an orthonormal basis for the (3-dimensional) space of the states of the system, since

$$\langle e_\ell, \vec{\lambda}(t)|e_{\ell'}, \vec{\lambda}(t)\rangle = \delta_{\ell,\ell'} \quad \forall t\,. \tag{23}$$

As a consequence of Eq.(23), at any time t the state of the system $|\psi(t)\rangle$ may be fully decomposed in the basis of adiabatic eigenstates of the system as

$$|\psi(t)\rangle = \sum_{\ell=1}^{3} \exp\left[-\mathrm{i}\int_0^t \mathrm{d}\tau\, E_\ell(\tau)\right] c_\ell(t)|e_\ell, \vec{\lambda}(t)\rangle\,. \tag{24}$$

By imposing to $|\psi(t)\rangle$ in Eq.(24) to obey the Schrödinger equation, we eventually obtain the time evolution of the c'_ℓ's in the adiabatic approximation

$$c_\ell(t) = \exp\left[-\int_0^t \mathrm{d}\tau \langle e_\ell, \vec{\lambda}(\tau)| \frac{\mathrm{d}}{\mathrm{d}\tau} |e_\ell, \vec{\lambda}(\tau)\rangle\right] c_\ell(0)\,. \tag{25}$$

From Eq.(25) we find that adiabaticity implies that, if the system undergoes a cycle in parameter space, starting from one of the states $|e_\ell, \vec{\lambda}(t)\rangle$, it ends up in the same state, with an extra phase given by the sum of the usual "dynamical" contribution $\Gamma_d = -E_\ell T$, and of a "geometrical", Berry phase, Γ_ℓ, given by

$$\Gamma_\ell = -\int_0^T \mathrm{d}t\, \mathrm{Im}\langle e_\ell, \vec{\lambda}(t)| \frac{\mathrm{d}}{\mathrm{d}t} |e_\ell, \vec{\lambda}(t)\rangle = -\oint_{\mathcal{C}} \mathrm{Im}\langle e_\ell, \vec{\lambda}|\mathrm{d}|e_\ell, \vec{\lambda}\rangle, \tag{26}$$

where d means usual differentiation with respect to $\vec{\lambda}$.

In our case, explicit calculation of Γ_ℓ gives

$$\Gamma_\ell = 2\pi|g|^2(C_\ell)^2\,. \tag{27}$$

In Fig.4, we report the eigenvalues of the adiabatic Hamiltonian as a function of b, for $r = \sqrt{|g|^2 + e^2}$, with $|g| = e$. In Fig.5, we show the Berry phase calculated, according to Eq.(27), for the lowest-energy state E_3. By looking at the figures. we see that, the situation is completely different, according to whether $b < 0$, or $b > 0$. Indeed, for $b < 0$, the lowest energy level E_3 is clearly nondegenerate, and the intermediate energy level (E_2) lies much higher in energy than E_3 (and close to E_1). As a consequence, the Berry phase goes down to zero. On the other hand, for $b > 0$, the two almost degenerate levels coincide with E_3 and E_2. Therefore, it is natural to expect a Berry phase to appear, in this case [11].

In Fig.(5), we see that the Berry phase Γ_3 converges to π, for large enough b. This can be understood by computing the approximate form of the adiabatic state

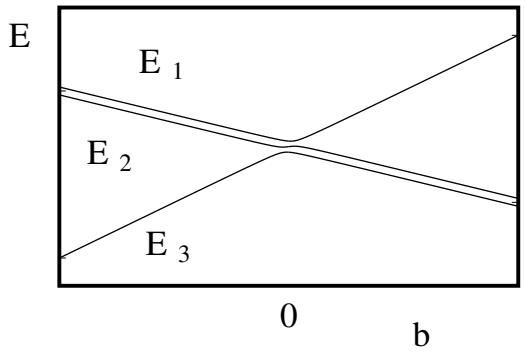

Fig. 4. Energy levels E_1, E_2, E_3 of the model Hamiltonian of Eq.(16) vs. b for $-1 \leq b \leq 1$; $r = 0.1$.

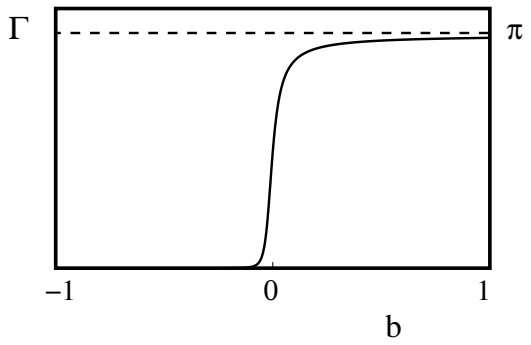

Fig. 5. Γ_3 vs. b for $-1 \leq b \leq 1$ and for $r = 0.1$.

$|e_3, \vec{\lambda}\rangle$ for $b/r \gg 1$. Indeed, from Eq.(21), one obtains

$$|e_3, \vec{\lambda}\rangle \underset{b/r \gg 1}{\longrightarrow} \frac{1}{\sqrt{2}} \begin{bmatrix} \mathrm{e}^{-\mathrm{i}(2\pi t)/T} \\ 0 \\ 1 \end{bmatrix}, \tag{28}$$

that provides a Berry phase Γ_3 equal to π.

The particular features of Γ_3 in Fig.5 are peculiar of the device we are dealing with. Remarkably, we may see that the device we describe works, somehow, as a "phase switcher". Indeed, for $b < 0$ the switcher is "off", and basically no phase is generated at the dot upon cycling in parameter space. On the other hand, as soon as b gets > 0, the switcher turns "on", a finite Berry phase is generated at the dot, and the phase itself keeps $\sim \pi$ as b/r becomes large enough [1]). Such a behavior might suggest of using a device like this as a possible solid-state qubit.

[1]) The apparent discrepancy with the result reported in [12] is due to a factor 2 missing in that paper.

However, in order to use it like so, one has to design an efficient way of reading out the dot's phase. In [12], for instance, it is proposed to capacitively couple the dot to one arm of an interferometric ring. Electrons travelling through the arm of the ring coupled to the quantum dot "read out" the phase at the dot. A measurement of DC conductance across the ring should, therefore, contain an interference term, depending upon Berry phase. Detecting, or not, such a contribution to the total DC conductance, should be an efficient way of probing whether, or not, a Berry phase has aroused at the quantum dot. This proposal for detecting the Berry phase at the quantum dot is briefly described in the next section.

5 Reading out the Berry phase at the quantum dot

In order to ensure an effective "phase readout" by the travelling electron, the actual coupling between dot and arm must be extended in space. This should correspond to an effective interaction Hamiltonian in the form [12]

$$H_{\mathrm{d-ring}} = q(t) \int \mathrm{d}x\, f(x) \Psi^{\dagger}(x) \Psi(x)\,, \tag{29}$$

where $q(t)$ is the charge operator at the quantum dot, $\Psi(x)$ is the field of the itinerant electrons, so that $\Psi^{\dagger}(x)\Psi(x)$ is the total charge density in the ring's arm, $f(x)$ is a smooth function, of support L, describing the coupling between dot and arm [2]).

Deriving in detail all possible interaction terms arising from the Hamiltonian in Eq.(29) requires going through a long and boring sequence of calculations. In fact, it is more useful to trade $H_{\mathrm{d-ring}}$ fir a much simpler, "toy" Hamiltonian H_W, which, nevertheless, is capable of catching the relevant physical aspects of the problem. In deriving H_W, it comes out to be useful to resort to chiral Fermionic modes, obtained expanding $\Psi(x)$ about the Fermi points at $\pm k_F$. In particular, by taking into account only long wavelength excitations about the Fermi surface, one obtains

$$\Psi(x) \approx \mathrm{e}^{\mathrm{i}k_F x}\psi_L(x) + \mathrm{e}^{-\mathrm{i}k_F x}\psi_R(x)\,. \tag{30}$$

The free Hamiltonian for the chiral Fermionic fields is

$$H_0 = \int \mathrm{d}k\, \frac{v_F}{2\pi}\, k \left[\psi_L^{\dagger}(k)\psi_L(k) + \psi_R^{\dagger}(k)\psi_R(k)\right], \tag{31}$$

while H_W takes the form

$$\begin{aligned} H_W \,=\, & \dot{\Phi}(t) \int_{-L/2}^{L/2} \mathrm{d}x \left[\psi_L^{\dagger}(x)\psi_L(x) - \psi_R^{\dagger}(x)\psi_R(x)\right] + \\ & + v_{\chi}(t) \int_{-L/2}^{L/2} \mathrm{d}x \left[\mathrm{e}^{2\mathrm{i}\Phi(t)}\psi_L^{\dagger}(x)\psi_R(x) + \mathrm{e}^{-2\mathrm{i}\Phi(t)}\psi_R^{\dagger}(x)\psi_L(x)\right] \equiv \\ & \equiv V_{\Phi}(t) + V_{\chi}(t)\,. \end{aligned} \tag{32}$$

[2]) For simplicity, we neglect spin henceforth

The function $\Phi(T)$ is related to the Berry phase Γ_3. In general, however, the relation between the two of them is quite involuted, due to nondynamical effects, that spoil adiabaticity of the whole procedure. The relevant thing is, however, that, if there is no Berry phase then $\Phi(t) = 0$, and vice versa. If the time evolution of $\Phi(t)$ is smooth enough, we may get rid of the potential $V_\Phi(t)$ by reabsorbing it in the chiral fields as

$$\psi_L(x,t) \to \mathrm{e}^{\mathrm{i}\Phi(t)}\psi_L(x,t)\,, \qquad \psi_R(x,t) \to \mathrm{e}^{-\mathrm{i}\Phi(t)}\psi_R(x,t)\,. \tag{33}$$

The rephasing of the chiral field operators in Eq.(33) implies a rephasing of the corresponding Green functions $G_{XY}(x,t;x',t')$ $(X,Y = L,R)$, by a phase factor depending on $\Phi(t)$. For instance, for the LL Green function one gets

$$G_{LL}(x,t;x',t') \to G_{LL}(x,t;x',t')\mathrm{e}^{\mathrm{i}[\Phi(t)-\Phi(t')]}\,, \tag{34}$$

and similar expressions for all the other relevant Green functions.

Because of the extra factor appearing in the Green functions and, therefore, in the transmission amplitudes across the ring's arm, one may infer that, at $\Phi \neq 0$, the total DC conductance across the ring, G, is given by

$$G[\Phi] = G[\Phi = 0] \cdot \tfrac{1}{2} \cdot \overline{[1 + \cos(\Phi(t+T) - \Phi(t))]}\,, \tag{35}$$

where $\overline{X(t)}$ denotes averaging $X(t)$ in time over a period T.

We are grateful to E. Kochetov for useful discussions.

Appendix: su(3)-algebra

In this appendix we recall the 3×3 hermitean matrices giving Gell-Mann representation of SU(3)-generators [3]). They are given by

$$\mathbf{T}_1 = \begin{bmatrix} 0 & 1 & 0 \\ 1 & 0 & 0 \\ 0 & 0 & 0 \end{bmatrix}, \qquad \mathbf{T}_2 = \begin{bmatrix} 0 & -\mathrm{i} & 0 \\ \mathrm{i} & 0 & 0 \\ 0 & 0 & 0 \end{bmatrix}, \qquad \mathbf{T}_3 = \begin{bmatrix} 1 & 0 & 0 \\ 0 & -1 & 0 \\ 0 & 0 & 0 \end{bmatrix},$$

$$\mathbf{T}_4 = \begin{bmatrix} 0 & 0 & 1 \\ 0 & 0 & 0 \\ 1 & 0 & 0 \end{bmatrix}, \qquad \mathbf{T}_5 = \begin{bmatrix} 0 & 0 & -\mathrm{i} \\ 0 & 0 & 0 \\ \mathrm{i} & 0 & 0 \end{bmatrix}, \qquad \mathbf{T}_6 = \begin{bmatrix} 0 & 0 & 0 \\ 0 & 0 & 1 \\ 0 & 1 & 0 \end{bmatrix},$$

$$\mathbf{T}_7 = \begin{bmatrix} 0 & 0 & 0 \\ 0 & 0 & -\mathrm{i} \\ \mathrm{i} & 0 & 0 \end{bmatrix}, \qquad \mathbf{T}_8 = \frac{1}{\sqrt{3}} \begin{bmatrix} 1 & 0 & 0 \\ 0 & 1 & 0 \\ 0 & 0 & -2 \end{bmatrix}.$$

The commutators among Gell-Mann matrices are formally given by

$$[\mathbf{T}_a, \mathbf{T}_b] = 2\mathrm{i}\sum_{c=1}^{8} f_{abc}\,\mathbf{T}_c$$

[3]) The results of this Appendix are reported from Appendix A of Ref. [13]

with

$$f_{123} = 1\,, \quad f_{458} = f_{678} = \frac{\sqrt{3}}{2}\,, \quad f_{147} = f_{246} = f_{257} = f_{345} = f_{516} = f_{637} = \frac{1}{2}\,.$$

The anticommutators, instead, are given by

$$\{\mathbf{T}_a, \mathbf{T}_b\} = \frac{4}{3}\,\delta_{ab} + 2\sum_{c=1}^{8} d_{abc}\,\mathbf{T}_c$$

with

$$d_{118} = d_{228} = d_{338} = -d_{888} = \frac{1}{\sqrt{3}}\,, \quad d_{448} = d_{558} = d_{668} = d_{778} = -\frac{1}{2\sqrt{3}}\,,$$
$$d_{146} = d_{157} = -d_{247} = d_{256} = d_{344} = d_{355} = -d_{366} = -d_{377} = \frac{1}{2}\,.$$

References

[1] S. Washburn and R.A. Webb: Rep. Prog. Phys. **55** (1992) 1311.

[2] Y. Aharonov and D. Bohm: Phys. Rev. **115** (1959) 485.

[3] F.E. Meijer, A.F. Morpurgo, T.M. Klapwijk, T. Koga and J. Nitta: `cond-mat/0406106`;
J.B. Miller, D.M. Zumbühl, C.M. Marcus, Y.B. Lyanda-Geller, D. Goldhaber-Gordon, K. Campman and A.C. Gossard: Phys. Rev. Lett. **90** (2003) 076807;
P. Lucignano, B. Jouault and A. Tagliacozzo: Phys. Rev. B **69** (2004) 045314;
P. Lucignano, B. Jouault, A. Tagliacozzo and B.L. Altshuler: Phys. Rev. B **71** (2005) 121310(R).

[4] R. Landauer: IBM J. Res. Dev. **1** (1957) 223;
M. Buttiker: IBM J. Res. Dev. **32** (1988) 317.

[5] R. Capozza, D. Giuliano, P. Lucignano and A. Tagliacozzo: accepted for Phys. Rev. Lett. (2005), `cond-mat/0505273`.

[6] F.D.M. Haldane: Phys. Rev. Lett. **50** (1983) 1153.

[7] D. Frustaglia and K. Richter: Phys. Rev. B **69** (2004) 235310.

[8] J. Nitta, T.Koga and F.E. Meijer: Physica E **18** (2003) 143;
F.E. Meijer, J. Nitta, T. Koga, A.F. Morpurgo and T.M. Klapwijk: Physica E **22** (2004) 402;
M.J. Yang, C.H. Yang, K.A. Cheng and Y.B. Lyanda-Geller: `cond-mat/0208260`.

[9] J.B. Yau, E.P. de Poortere and M. Shayegan: Phys. Rev. Lett. **88** (2002) 146801; **90** (2003) 119702; **90** (2003) 119704;
A.G. Mal'shukov and K.A. Chao: Phys. Rev. Lett. **90** (2003) 119701;
A.G. Wagh and V.C. Rakhecha: Phys. Rev. Lett. **90** (2003) 119703.

[10] A.G. Wagh and V.C. Rackhecha: Phys. Rev. A **48** (1993) 1729(R).

[11] M.V. Berry: Proc. R. Soc. London, Ser.A **392** (1984) 45.

[12] D. Giuliano, P. Sodano and A. Tagliacozzo: Phys. Rev. B **67** (2003) 155317.

[13] E. Ercolessi, G. Marmo, G. Morandi and N. Mukunda: Int. Jour. Mod. Phys. A **16** (2001) 5007.